Available online at www.sciencedirect.com
SCIENCE DIRECT®
Journal of Catalysis 221 (2004) 335–346
JOURNAL OF CATALYSIS
www.elsevier.com/locate/jcat

Synthesis of Pd/SiO_2, Ag/SiO_2, and Cu/SiO_2 cogelled xerogel catalysts: study of metal dispersion and catalytic activity

Stéphanie Lambert,[a] Caroline Cellier,[b] Paul Grange,[b] Jean-Paul Pirard,[a] and Benoît Heinrichs [a,*]

[a] *Laboratoire de Génie Chimique, B6a, Université de Liège, B-4000 Liège, Belgium*
[b] *Unité de Catalyse et chimie des matériaux divisés, Université Catholique de Louvain, B-1348 Louvain-La-Neuve, Belgium*

Received 23 May 2003; revised 22 July 2003; accepted 22 July 2003

Abstract

Pd/SiO_2, Ag/SiO_2, and Cu/SiO_2 xerogel catalysts have been synthesized by cogelation of tetraethoxysilane (TEOS) and chelates of Pd, Ag, and Cu with 3-(2-aminoethylamino)propyltrimethoxysilane (EDAS). It appears that the metal complex acts as a nucleation agent in the formation of silica particles. The resulting catalysts are then composed of completely accessible metallic crystallites with a diameter of about 3 nm located inside silica particles exhibiting a monodisperse microporous distribution. The metal dispersion has been determined from CO and O_2 chemisorption, TEM, and X-ray diffraction. Although metallic particles are located inside silica particles, their complete accessibility, via the micropore network, has been shown. 1,2-Dichloroethane hydrodechlorination over Pd/SiO_2 catalysts mainly produces ethane and the specific hydrodechlorination rate per gram of Pd decreases when metal loading increases. Hydrodechlorination over Pd/SiO_2 catalysts is a structure-insensitive reaction with regard to the ensemble size concept. Benzene oxidation over Ag/SiO_2 and Cu/SiO_2 catalysts produces H_2O and CO_2 only and specific oxidation rate per gram of metal decreases when silver and copper loadings increase. Furthermore, it is concluded that benzene oxidation is a structure-insensitive reaction.

Keywords: Cogelled xerogel catalysts; Nucleation; Metal dispersion; Hydrodechlorination; Oxidation

1. Introduction

A high activity of a supported catalyst often calls for a large active surface area and, thus, for small particles, i.e., a high dispersion of the active phase. Because small metal particles tend to sinter already at relatively low temperatures, these generally are applied into a support material which itself is thermally stable and maintains a high specific surface area up to high temperatures [1]. With a support like silica, other important physical features like texture (specific surface area, pore size distribution, and porous volume), density, and mechanical strength can be established.

The sol–gel method was used by several authors in order to obtain monometallic catalyst particles finely dispersed on a mineral support. Schubert and co-workers developed a particularly interesting method to homogeneously disperse nanometer-sized metal particles in a silica matrix [2–5]. These authors used alkoxides of the type $(RO)_3Si–X–A$ in which a functional organic group A, able to form a chelate with a cation of a metal such as palladium, silver, copper, nickel, etc. is linked to the hydrolyzable silyl group $(RO)_3Si–$ via an inert and hydrolytically stable spacer X. The cocondensation of such molecules with a network-forming reagent such as TEOS, $Si(OC_2H_5)_4$, results in materials in which the metal is anchored to the SiO_2 matrix.

Heinrichs et al. used this cogelation method for the preparation of Pd/SiO_2 aerogel catalysts [6]. In this study, $(RO)_3Si–X–A$ = 3-(2-aminoethylamino)propyltrimethoxysilane, $NH_2–CH_2–CH_2–NH–(CH_2)_3–Si(OCH_3)_3$ = EDAS, and the Pd precursor is Pd acetylacetonate, $Pd[CH_3COCH=C(O–)CH_3]_2 = Pd(acac)_2$. It has been shown that the Pd^{2+} complex, $Pd^{2+}[NH_2–CH_2–CH_2–NH–(CH_2)_3–Si(OCH_3)_3]_2$, acts as a nucleation agent in the formation of silica particles. The resulting catalysts are composed of completely accessible palladium crystallites located inside silica particles. It was shown that these samples are sinterproof during hypercritical drying due to the fact that Pd crystallites cannot migrate because they are trapped inside the microporous SiO_2 particles. In such catalysts, in order to reach active

* Corresponding author.
E-mail address: b.heinrichs@ulg.ac.be (B. Heinrichs).

0021-9517/$ – see front matter
doi:10.1016/j.jcat.2003.07.014

sites, reactants must first diffuse through large pores located between aggregates of SiO_2 particles and then through smaller pores between those elementary particles inside the aggregates. Finally, they diffuse through micropores inside the silica particles. It was shown that there is no problem of mass transfer at each of the three levels [7].

TEM micrographs obtained for Pd/SiO_2 catalysts [6] show palladium particles located inside microporous silica particles. It was suggested that this localization of the palladium inside the silica particles was induced by a nucleation process initiated by the ligand of the palladium, EDAS. Due to the hydrolyzable functions of EDAS, Si–O–Si bonds can form all around the $Pd^{2+}(EDAS)_2$ complex. The fact that gelation occurs in half an hour in the presence of EDAS, whereas it would take days without EDAS under the same conditions, indicates that EDAS reacts faster than TEOS [8]. It has been shown that this acceleration is caused by methoxy groups contained in EDAS, which are more reactive than ethoxy groups contained in TEOS. So hydrolyzed EDAS molecules can act as a nucleation agent leading to silica particles with a hydrolyzed EDAS core and a shell principally made of hydrolyzed TEOS. The relation between diameter of SiO_2 particles and TEOS and EDAS concentrations has been studied [6,8–11] and established the validity of the nucleation model by EDAS.

Although the sol–gel method for metallic cogelled catalysts had been developed in previous papers, for the first time in this study are presented very important relationships existing among textural properties, metallic dispersion, and catalytic activity in xerogel catalysts. Another purpose of the present study is to generalize the cogelation method for the preparation of xerogel catalysts containing a metal such as palladium, silver, or copper. Moreover, this study checks if all textural and catalytic properties observed with xerogels without metal [8–11] and Pd/SiO_2 aerogel catalysts [6] are conserved with other metals in these xerogel catalysts. So the dispersion, localization, and accessibility of different metals in cogelled xerogels are examined by using techniques such as nitrogen adsorption isotherms, mercury porosimetry, helium pycnometry, transmission electron microscopy (TEM), chemisorption measurements, X-Ray diffraction (XRD), and catalytic tests. Finally, the nucleation phenomenon by the metal complex in the formation of silica particles is examined.

2. Experimental

2.1. Catalyst preparation

2.1.1. Gel synthesis

Six Pd/SiO_2, five Ag/SiO_2, and seven Cu/SiO_2 catalysts were prepared in ethanol from the corresponding metal precursor, $Pd(acac)_2$ ($Pd[CH_3COCH{=}C(O–)CH_3]_2$), Ag(OAc) ($Ag[CH_3CO(O–)]$), $Cu(OAc)_2$ ($Cu[CH_3CO(O–)]_2$), TEOS ($Si(OC_2H_5)_4$), EDAS ($NH_2–CH_2–CH_2–NH–(CH_2)_3–Si(OCH_3)_3$), and 0.18 N NH_3 aqueous solution (pH 11.2). In those syntheses, $Pd(acac)_2$ or Ag(OAc) or $Cu(OAc)_2$ was mixed with EDAS in half of the total ethanol volume (EDAS/$Pd(acac)_2$ molar ratio = 2, EDAS/Ag(OAc) molar ratio = 2, and EDAS/$Cu(OAc)_2$ molar ratio = 4). The slurry was stirred at room temperature until clear yellow, colorless, and clear blue solution was obtained for Pd, Ag, and Cu, respectively (about half an hour). After addition of TEOS, a 0.18 N NH_3 aqueous solution (pH 11.2) in the remaining half of the total ethanol volume was added to the mixture under vigorous stirring. The volume of the final solution was 170 ml. The hydrolysis ratio, that is, the molar ratio $H = [H_2O]/([TEOS] + \frac{3}{4}[EDAS])$, and the dilution ratio, that is, the molar ratio $R = [\text{ethanol}]/([TEOS] + [EDAS])$ were kept constant at values of 5 and 10, respectively, for all samples. Although Pd/SiO_2, Ag/SiO_2 and Cu/SiO_2 catalysts were prepared in ethanol and although that pH is defined in aqueous solution only, the pH of the alcoholic solution was measured for all series 5 min after introduction of the last reactive component. The pH values observed are between 10.4 and 10.7. It is assumed that those slight variations are negligible. The vessel was then tightly closed and heated up to 70 °C for 3 days (gelling and aging [12]). Synthesis-operating variables of Pd/SiO_2, Ag/SiO_2, and Cu/SiO_2 catalysts are given in Table 1. Each sample is named by the corresponding metal (Pd, Ag, or Cu) followed by its actual weight percentage.

2.1.2. Drying

The wet gels were dried under vacuum according to the following procedure: the flasks were opened and put into a drying oven at 60 °C, and the pressure was slowly decreased (to prevent gel bursting) to reach the minimum value of 1200 Pa after 90 h. The drying oven was then heated at 150 °C for 72 h except for sample Pd7.3, which was heated at 150 °C for 144 h. The resulting samples are xerogels [12].

2.1.3. Calcination

The calcination conditions for Pd/SiO_2, Ag/SiO_2, and Cu/SiO_2 catalysts were as follows: the sample was heated up to 400 °C at a rate of 120 °C/h under flowing air (0.02 mmol s^{-1}); this temperature was then maintained for 12 h in air (0.1 mmol s^{-1}).

2.1.4. Reduction

The Pd/SiO_2 and Ag/SiO_2 catalysts were heated up to 350 °C at a rate of 350 °C/h under flowing H_2 (0.23 mmol s^{-1}) and maintained at this temperature for 3 h (same flow). The Cu/SiO_2 catalysts were heated up to 400 °C at a rate of 350 °C/h under flowing H_2 (0.23 mmol s^{-1}) and maintained at 400 °C for 4 h (same flow).

2.2. Catalyst characterization

Apparent densities [13] were measured by He pycnometry on a Micromeritics AccuPyc 1330. N_2 adsorption–

desorption isotherms were measured at 77 K on a Fisons Sorptomatic 1990 after outgassing for 24 h at ambient temperature. After a 2-h outgassing at ambient temperature, Hg porosimetry measurements were performed with sample monoliths using a manual porosimeter from 0.01 to 0.1 MPa and a Carlo Erba Porosimeter 2000 from 0.1 to 200 MPa.

SiO_2 and metal particles sizes were examined by transmission electron microscopy with a Philips CM100 microscope. All samples were impregnated with an epoxy resin (Epon 812) to which an amine was added to serve as a hardener. Hardening goes on for 72 h at 60 °C and 60-nm slices were then cut up with a Reichert-Jung Ultracut E microtome. Finally, these slices were put on a copper grid.

X-ray diffraction was also used to determine metal particles' sizes. Patterns were obtained with hand-pressed samples mounted on a Siemens D5000 goniometer using the Cu-K_α line (Ni filter).

Metal dispersion in Pd/SiO_2, Ag/SiO_2, and Cu/SiO_2 catalysts was determined from CO chemisorption at 30 °C on a Fisons Sorptomatic 1990 device and O_2 chemisorption at 150 °C for Ag and at 30 °C for Cu on a Micrometrics device, respectively. Before measurements, the calcined sample was reduced in situ in flowing H_2 (0.003 mmol s^{-1}) at 350 °C for 3 h for palladium and silver, and at 400 °C for 4 h for copper. After, this sample was outgassed under vacuum at 340 °C for 16 h for palladium and silver, and at 200 °C for 20 h for copper. A double adsorption method was used: (i) first adsorption isotherm was measured, which includes both physisorption and chemisorption; (ii) after a 2-h outgassing at 30 °C for CO or at 150 °C (Ag) or 30 °C (Cu) for O_2, a second isotherm was measured which includes physisorption only. Both isotherms are determined in the pressure range of 10^{-8} to 2×10^{-1} kPa. The difference between first and second isotherms gave the CO or O_2 chemisorption isotherm [14–16]. The latter theoretically exhibited a horizontal linear region corresponding to the complete coverage of metallic sites by a monolayer of adsorbate. However the linear region of experimental chemisorption isotherms often exhibited a slope and the monolayer uptake was obtained by back extrapolation of the linear region to zero pressure [15–22].

2.3. Catalytic experiments

2.3.1. 1,2-Dichloroethane hydrodechlorination ($ClCH_2$–$CH_2Cl + H_2$)

The six Pd/SiO_2 catalysts were tested for this reaction, which was conducted in a stainless-steel tubular reactor (internal diameter: 10 mm) at a pressure of 0.3 MPa. The reactor was placed in a convection oven. A constant flow of each reactant was maintained by a Gilson piston pump for $ClCH_2$–CH_2Cl and Brooks mass flow controllers for H_2 and He. The effluent was analyzed by gas chromatography (ThermoFinnigan with FID) using a Porapak Q5 packed column. Prior to each experiment, the Pd/SiO_2 catalyst was reduced in situ at atmospheric pressure in flowing H_2 (0.023 mmol s^{-1}) while being heated to 350 °C at a rate of 350 °C/h and was maintained at this temperature for 3 h. After reduction, the Pd/SiO_2 catalyst was cooled in H_2 to the desired initial reaction temperature of 300 °C. The total flow of the reactant mixture was 0.45 mmol s^{-1} and consisted of $ClCH_2$–CH_2Cl (0.011 mmol s^{-1}), H_2 (0.023 mmol s^{-1}), and He (0.42 mmol s^{-1}). The temperature was successively kept at 300 °C (10 h to allow activity stabilization after fast initial deactivation), 350 °C (2 h), and 300 °C (2 h). The effluent was analyzed every 15 min and eight analyses were made at each temperature (40 for the first level). For each catalytic experiment, the mass of catalyst pellets, sieved between 250 and 500 µm, was calculated so that 1,2-dichloroethane conversion was approximately equal to 10% at 300 °C.

2.3.2. Benzene oxidation

The five Ag/SiO_2 and four Cu/SiO_2 (Cu1.0, Cu1.5, Cu2.1, and Cu4.5) catalysts were tested for this reaction, which was conducted in a quartz tubular reactor (internal diameter: 3 mm) at atmospheric pressure. The reactor was placed in a tubular oven. A constant flow of each reactant was maintained by Brooks mass flow controllers for C_6H_6/N_2, O_2, and N_2. The reactants and products from a possible incomplete combustion were separated by gas chromatography (Chrompack column 773) and then quantified using a flame ionization detector (FID). The reactor feeding consisted in 0.007 mmol s^{-1} of C_6H_6/N_2 mixture (2550 ppm of benzene in nitrogen), 0.009 mmol s^{-1} of oxygen, and 0.048 mmol s^{-1} of nitrogen. Catalyst pellets (0.1 g) sieved between 0.2 and 0.315 mm were diluted in 7 cm^3 of glass beads with the same diameter, previously checked to be inactive. Prior to each experiment, the Ag/SiO_2 and Cu/SiO_2 catalysts were first activated and then stabilized. Activation was performed in situ at 150 °C, for 30 min, under flowing O_2 (0.009 mmol s^{-1}). Stabilization was obtained by letting the reaction take place at 150 °C for a period of 2 h at the end of which conversion reached an almost constant value. Then, conversion for Ag/SiO_2 and Cu/SiO_2 catalysts was measured at temperatures increasing by steps of 20 °C from 160 to 360 °C with three measurements every 15 min for each temperature.

3. Results

3.1. Synthesis

Synthesis operating variables of cogelled catalysts are given in Table 1.

Gel time is the time elapsed between the introduction of the last reactant in the solution and the gelation in the oven at 70 °C. Gelation is defined as the moment when the liquid does not flow anymore when the flask is tipped at an angle of 45°. The comparison between samples inside the three series indicates that, at low EDAS concentration and also at

Table 1
Synthesis operating variables, theorical and actual metal loading of Pd/SiO_2, Ag/SiO_2, and Cu/SiO_2 catalysts

Sample	n_m[a] (mmol)	n_{EDAS} (mmol)	n_{TEOS} (mmol)	n_{H_2O} (mmol)	n_{NH_3} (mmol)	$n_{C_2H_5OH}$ (mmol)	Gel time (min)	Theorical metal loading (wt%)	Weight loss[b] ±0.5% (wt%)	Actual metal loading ±0.1% (wt%)
Pd0.4	0.376	0.76	188	941	3.05	1890	80	0.35	5.5	0.38
Pd1.1	1.074	2.15	186	941	3.05	1890	30	1.01	10.0	1.11
Pd1.6	1.369	2.74	186	941	3.05	1890	28	1.28	19.5	1.57
Pd2.4	1.835	3.62	185	938	3.04	1890	26	1.72	31.0	2.45
Pd3.1	2.289	4.58	184	938	3.04	1890	26	2.15	31.5	3.07
Pd7.3	4.811	9.62	179	930	3.02	1890	22	4.52	40.5	7.26
Ag0.4	0.442	0.85	188	942	3.05	1890	170	0.42	5.5	0.44
Ag1.0	1.073	2.13	186	941	3.05	1890	51	1.02	2.5	1.04
Ag1.5	1.608	3.21	185	938	3.04	1890	50	1.53	1.5	1.54
Ag2.6	2.705	5.39	183	935	3.03	1890	50	2.58	0.0	2.58
Ag3.6	3.832	7.63	181	932	3.02	1890	52	3.65	0.0	3.65
Cu0.1	0.199	0.76	188	941	3.05	1890	150	0.11	4.0	0.12
Cu1.0	1.757	7.20	181	935	3.03	1890	69	0.99	2.5	1.00
Cu1.3	2.282	9.16	180	932	3.02	1890	62	1.28	2.0	1.29
Cu1.5	2.716	10.86	178	930	3.02	1890	54	1.52	1.0	1.53
Cu1.7	3.009	12.10	176	927	3.00	1890	53	1.69	1.0	1.70
Cu2.1	3.814	15.31	173	924	3.00	1890	49	2.14	0.0	2.14
Cu4.5	8.036	32.08	156	902	2.92	1890	47	4.52	0.0	4.52

[a] n_m, the metal precursor, is $Pd(acac)_2$ in Pd/SiO_2 catalysts, Ag(OAc) in Ag/SiO_2 catalysts, and $Cu(OAc)_2$ in Cu/SiO_2 catalysts.
[b] Weight loss $= 100 \times (m_{th} - m_a)/m_{th}$, where m_{th} is the theorical mass and m_a is the actual catalyst mass measured after drying, calcination, and reduction.

low metal precursor concentration since EDAS/metal precursor molar ratio is kept constant in each series, an increase in the EDAS and metal precursor concentrations decreases gel time. At higher EDAS and metal precursor concentrations, gel time tends to become less or nondependent on the amounts of those reactants.

The actual metal loading in cogelled catalysts is sometimes higher than theoretical loading because the actual catalyst mass after drying, calcination, and reduction is lower than theoretical mass. In fact, some TEOS and/or EDAS sometimes remains unreacted and is volatilized during drying. This theoretical mass (m_{th}) is calculated from

$$m_{th} = n_m M_m + (n_{TEOS} + n_{EDAS}) M_{SiO_2}, \quad (1)$$

where n_m is the amount of metal in the gel (mmol); M_m is the metal atomic weight; n_{TEOS} and n_{EDAS} are respectively the amount of TEOS and EDAS in the gel (mmol); M_{SiO_2} is the molecular weight of SiO_2, 60.085 g mol^{-1}. In this equation, it is assumed that all TEOS and EDAS molecules are converted into SiO_2. Results in Table 1 clearly show that, in all Ag/SiO_2 and Cu/SiO_2 catalysts, the weight loss decreases to 0% when the EDAS concentration increases. In Pd/SiO_2 catalysts, the behavior is different: the weight loss increases with EDAS concentration.

3.2. Dispersion and localization of metal

Table 2 gives metal particle size determined by TEM, by chemisorption of CO (Pd catalysts) or O_2 (Ag and Cu catalysts) and by XRD.

TEM analysis indicates that beyond a value of metal loading which is between 1 and 1.5 wt% in the three series (Pd/SiO_2, Ag/SiO_2, and Cu/SiO_2), all samples exhibit metal particles distributed in two families of different sizes: small crystallites between 2 and 4 nm and large crystallites between 10 and 30 nm (Fig. 1). In all catalysts, the mean diameter of small crystallites, d_{TEM1}, is the arithmetic mean of 50 diameters of small metal particles measured on TEM micrographs. When large crystallites are present, their number is much smaller than for small crystallites and their mean diameter, d_{TEM2}, is then estimated from an average of 3 to 20 crystallites. In each series, d_{TEM1} seems to decrease, whereas d_{TEM2} seems to increase when the metal loading increases. Concerning localization of metallic crystallites, it appears that cogelled catalysts are composed of silica particles arranged in strings or aggregates, and although TEM gives only a 2D view, it seems that small metal particles are located inside silica particles, whereas large metal particles are located at their surface (Fig. 1).

The mean size of metal particles has been also derived from metal dispersion, D, measured by CO chemisorption for Pd/SiO_2 catalysts and O_2 chemisorption for Ag/SiO_2 and Cu/SiO_2 catalysts. In the case of CO chemisorption over Pd, it is well known that the chemisorption mean stoichiometry $X_{Pd–CO}$, that is, the mean number of Pd atoms on which one CO molecule is adsorbed, depends on metal dispersion, D [23–27]. Joyal and Butt [26] have determined $X_{Pd–CO}$ as a function of dispersion in Pd/SiO_2 catalysts and their results are used in an iterative method developed in the present work to calculate metal dispersion in Pd/SiO_2 cogelled catalysts: (i) the starting value of 2 is used for $X_{Pd–CO}$ and a first value of D is calculated from the CO monolayer uptake; (ii) by means of the table established by Joyal and Butt [26], a new value of $X_{Pd–CO}$ is determined which corresponds to the precedent value obtained for D and that new value of

Table 2
Metal particle size and dispersion

Catalyst	Actual metal loading (wt%)	TEM				CO or O_2 chemisorption		XRD
		d_{TEM1} (nm)	σ_{TEM1} (nm)	d_{TEM2} (nm)	σ_{TEM2} (nm)	d_{chem} (nm)	D (%)	d_{XRD} (nm)
Pd0.4	0.38	3.0	0.4	–[a]	–[a]	2.8	40	–[b]
Pd1.1	1.11	2.7	0.2	–[a]	–[a]	2.6	44	–[b]
Pd1.6	1.57	2.7	0.2	11	1	3.0	36	4
Pd2.4	2.45	2.6	0.2	15	2	4.0	28	7
Pd3.1	3.07	2.3	0.3	18	4	4.6	24	11
Pd7.3	4.52	2.5	0.3	24	7	7.0	16	17
Ag0.4	0.44	4.0	0.5	–[a]	–[a]	4.2	28	–[b]
Ag1.0	1.04	3.6	0.3	–[a]	–[a]	4.8	24	–[b]
Ag1.5	1.54	3.3	0.3	13	6	5.8	20	7
Ag2.6	2.58	3.2	0.3	20	5	7.4	16	10
Ag3.6	3.65	2.9	0.2	30	8	9.8	12	14
Cu0.1	0.12	4.2	0.6	–[a]	–[a]	–[b]	–[b]	–[b]
Cu1.0	1.00	3.2	0.4	–[a]	–[a]	3.8	28	–[b]
Cu1.3	1.29	3.3	0.4	–[a]	–[a]	3.8	28	–[b]
Cu1.5	1.53	3.1	0.4	8	2	5.2	20	12
Cu1.7	1.70	3.1	0.3	10	2	6.4	16	12
Cu2.1	2.14	2.8	0.2	15	6	6.4	16	18
Cu4.5	4.52	2.4	0.2	30	9	8.6	12	24

d_{TEM1}, d_{TEM2}, mean diameters of small and large metal particles, respectively, measured by TEM; σ_{TEM1}, σ_{TEM2}, standard deviations associated with d_{TEM1} and d_{TEM2}, respectively; D, metal dispersion measured by chemisorption; d_{chem}, mean diameter derived from dispersion D; d_{XRD}, mean size of metal particles estimated from X-ray line broadening.

[a] Not observed.

[b] Not measurable.

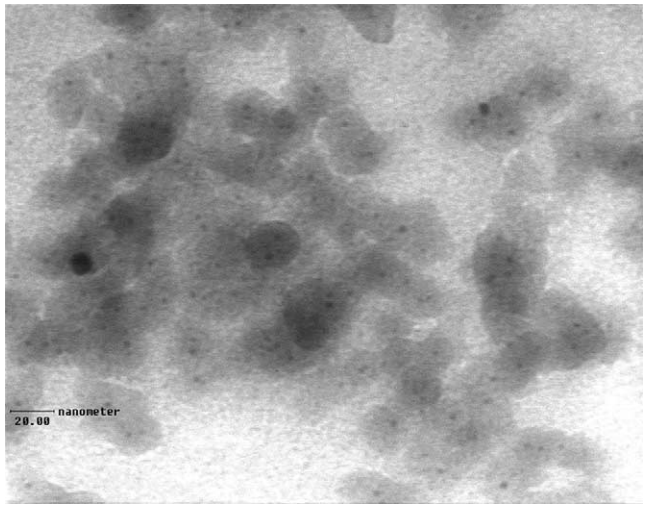

Fig. 1. TEM micrograph of Ag2.6 sample (500,000×).

$X_{Pd–CO}$ is used to calculate a new value of D; (iii) the cycle is repeated until convergence.

In the case of O_2 chemisorption over Ag, Czanderna [28] and Sachtler et al. [29] suggested that the initial adsorption of oxygen on a clean silver surface is a dissociative adsorption of an oxygen molecule on an ensemble of four adjacent silver atoms. This result was also checked by Wang et al. [30]. Therefore, the dispersion of silver in Ag/SiO_2 cogelled catalysts is calculated from the O_2 monolayer uptake with a value of 4 for $X_{Ag–O_2}$, which is the number of Ag atoms on which one O_2 molecule is adsorbed. In the case of O_2 chemisorption over Cu, Vasilevich et al. [31] suggested that one oxygen atom is joined with two surface copper atoms, in accordance with the formula Cu_2O. Therefore, the dispersion of copper in Cu/SiO_2 cogelled catalysts is calculated from the O_2 monolayer uptake with a value of 4 for $X_{Cu–O_2}$, which is the number of Cu atoms on which one O_2 molecule is adsorbed. During O_2 chemisorption measurements over Ag/SiO_2 and Cu/SiO_2 catalysts, it is important to avoid the formation of silver or copper bulk oxide, which could strongly falsify the dispersion calculation. This has been checked by examining Ag and Cu cogelled catalysts by XRD after O_2 chemisorption. No oxide phase is observed which indicates that bulk oxidation has been avoided. Dispersion values are given in Table 2.

A mean diameter, d_{chem}, of Pd, Ag, and Cu crystallites has been derived from dispersion values assuming those crystallites to be roughly spherical in shape. Values of d_{chem} are given in Table 2. In each series, it is observed that D decreases, and so d_{chem} increases, when the metal loading increases. Moreover, at comparable metal loadings, higher dispersions are reached with Pd catalysts in comparison with Ag and Cu catalysts, the latter exhibiting similar values. One has to note the agreement between TEM and chemisorption for samples containing, according to TEM analysis, one single family of particle size. In the case of sample containing two families of particle size, values of d_{chem} are between d_{TEM1} and d_{TEM2}.

X-ray diffraction is the third experimental technique that has been used to evaluate the size of metal crystallites. A mean size, d_{XRD}, has been calculated from Scherrer's formula based on line broadening analysis (Table 2) [19].

A comparison among d_{XRD}, d_{TEM1}, and d_{TEM2} in Table 2 shows that XRD and TEM results are in agreement since d_{XRD} values are between d_{TEM1} and d_{TEM2} values. However, the mean diameter estimated from XRD, d_{XRD}, is always higher than the mean diameter estimated from chemisorption, d_{chem}. As explained by Bergeret and Gallezot [19], this is due to the fact that d_{XRD} corresponds to a volume-weighted average diameter, $d_v = \sum n_i d_i^4 / \sum n_i d_i^3$, whereas d_{chem} corresponds to a surface-weighted average diameter, $d_s = \sum n_i d_i^3 / \sum n_i d_i^2$ (n_i is the number of metal particles of a given diameter d_i). In consequence, d_{XRD} gives more weight to the larger particles than d_{chem}, which explains that d_{XRD} values are higher than d_{chem} values.

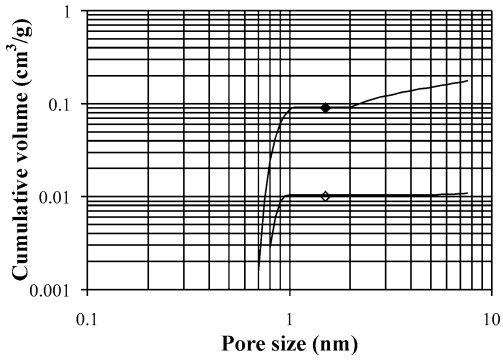

Fig. 2. Pore-size distributions of fresh Ag3.6 (◆) and tested Ag3.6 (◇) samples.

3.3. Texture of catalysts

The main textural properties of all samples are given in Table 3.

The catalyst apparent density, ρ_{app}, that is, the density including closed pores according to IUPAC [13], has been measured by helium pycnometry. Values given in Table 3 are very close to the true density, that is, the density excluding pores according to IUPAC, of dried alkoxy-derived silica gels, that is 2.2 g/cm^3 [32].

Pore-size distributions over the micro- and mesopore size range are shown in Fig. 2 for fresh Ag3.6 sample, for example, because all fresh Pd/SiO_2, Ag/SiO_2, and Cu/SiO_2 catalysts present the same trends over the micro- and mesopore size range. These curves were obtained by applying a combination of various methods to their respective validity domains and by adding the porous volumes corresponding to each domain [8–11]. Examination of Fig. 2 shows that Ag3.6 sample is characterized by a steep volume increase around 0.8 nm followed by a plateau.

Table 3
Sample textural properties

Sample	ρ_{app} (g/cm^3)	V_v (cm^3/g)	S_{BET} (m^2/g)	d_{SiO_2} (nm)	σ_{SiO_2} (nm)
Pd0.4	2.070	5.0	315	28.9	2.4
Pd1.1	2.092	3.2	365	19.5	1.3
Pd1.6	2.192	2.8	370	17.9	1.5
Pd2.4	2.220	2.6	475	15.1	1.0
Pd3.1	2.188	2.5	495	12.9	1.3
Pd7.3	2.256	2.0	570	9.8	1.5
Ag0.4	2.112	5.5	200	33.4	1.8
Ag1.0	2.206	5.4	260	24.8	1.0
Ag1.5	2.196	4.2	280	21.6	1.3
Ag2.6	2.174	3.0	375	17.7	1.7
Ag3.6	2.234	2.8	465	15.3	1.9
Cu0.1	2.110	7.3	245	> 60	4.8
Cu1.0	2.108	3.4	285	48.2	4.4
Cu1.3	2.190	3.3	365	43.7	3.2
Cu1.5	2.226	2.9	395	34.3	3.7
Cu1.7	2.188	2.7	410	30.0	3.3
Cu2.1	2.200	2.4	460	23.5	2.6
Cu4.5	2.238	1.3	570	16.7	1.1

ρ_{app}, apparent density measured by helium pycnometry; V_v, total cumulative specific pore volume; S_{BET}, specific surface area obtained by BET method; d_{SiO_2}, silica particle diameter measured by TEM; σ_{SiO_2}, standard deviation associated with d_{SiO_2}.

It is observed from Table 3 that the total pore volume, V_v, that is, the pore volume obtained by addition of pore volume measured by mercury porosimetry and cumulative volume of micropores and pores of width between 2 and 7.5 nm measured by N_2 adsorption-desorption [8–11], decreases and the specific surface area, S_{BET}, increases as the metal content and therefore the amount of EDAS in the catalyst increases in all series.

Texture and morphology of cogelled catalysts have been also examined by TEM and the size of SiO_2 elementary particles, d_{SiO_2}, has been evaluated. Sizes given in Table 3 represent the arithmetic mean of 50 particles. It is observed in the three series that d_{SiO_2} decreases as the metal loading and therefore the amount of EDAS in the catalyst increases (Table 3).

3.4. Catalytic experiments

It has been shown in a previous paper [7] that because of the very particular structure of those catalysts diffusional limitations are avoided. Indeed, in Pd/SiO_2, Ag/SiO_2, and Cu/SiO_2 xerogel catalysts, in order to reach active sites, reactants must first diffuse through large pores located between aggregates of SiO_2 particles and then through smaller pores between those elementary particles inside the aggregates. Finally, they diffuse through micropores inside the silica particles. It was shown that there is no problem of mass transfer at each of the three levels. The Weisz modulus, which compares the observed reaction rate to the diffusion rate, has a value much smaller than 1 at three discrete levels (macroscopic pellet, aggregate of silica particles, and elementary silica particle containing an active metallic crystallite). So there are no pore diffusion limitations and the observed rate r is equal to the intrinsic rate of the chemical reaction.

3.4.1. 1,2-Dichloroethane hydrodechlorination over Pd/SiO_2 catalysts

In Fig. 3, conversion as well as C_2H_6, C_2H_4, and C_2H_5Cl selectivities are given as a function of time and temperature over Pd1.1, for example. In fact, the results are the same for all Pd/SiO_2 samples because as noted under Experimental, the mass of catalyst pellets has been adjusted for each sample in order to obtain similar conversions between 10 and 20%. This has been done so as to allow a comparison of selectivities from one sample to another.

All Pd/SiO_2 catalysts mainly produce ethane, C_2H_6, with a selectivity between 70 and 90%. Two secondary products are observed: ethyl chloride, C_2H_5Cl, and ethylene, C_2H_4. In each case, a temperature increase from 300 to 350 °C is beneficial to C_2H_4 selectivity and detrimental to C_2H_6 and C_2H_5Cl selectivities. The examination of conversion curves shows that a deactivation, which is faster at the beginning of the catalytic test and when the temperature increases, is observed with all samples.

The consumption rate of 1,2-dichloroethane r is calculated from chromatographic measurements of C_2H_6, C_2H_5Cl, and C_2H_4 concentrations in the reactor effluent and from the differential reactor equation that is written as

$$r = \frac{F_A + F_{Cl} + F_E}{W} \quad (F_{A0}, F_{Cl0}, \text{ and } F_{E0} = 0), \qquad (2)$$

where r is the consumption rate (mmol kg_{Pd}^{-1} s^{-1}), F_A is the molar flow rate of ethane at the reactor outlet (mmol s^{-1}), F_{A0} is the molar flow rate of ethane at the reactor inlet (mmol s^{-1}), F_{Cl} is the molar flow rate of ethyl chloride at the reactor outlet (mmol s^{-1}), F_{Cl0} is the molar flow rate of ethyl chloride at the reactor inlet (mmol s^{-1}), F_E is the molar flow rate of ethylene at the reactor outlet (mmol s^{-1}), F_{E0} is the molar flow rate of ethylene at the reactor inlet (mmol s^{-1}), and W is the palladium mass inside the reactor (kg_{Pd}).

For all Pd/SiO_2 catalysts, r has been calculated from Eq. (2) at the temperatures of 300 and 350 °C, and these results are presented as a function of palladium loading in Fig. 4. It is observed that r increases when the palladium loading decreases.

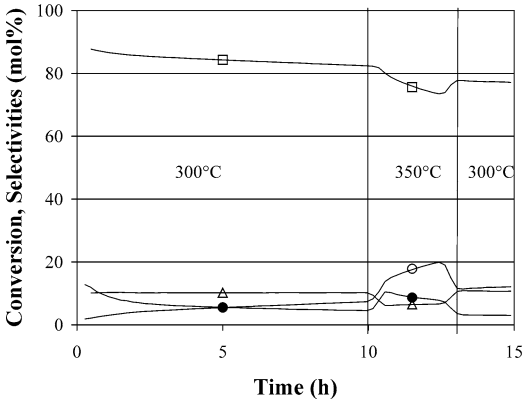

Fig. 3. Hydrodechlorination of 1,2-dichloroethane over Pd1.1 sample. (●) $ClCH_2$–CH_2Cl conversion, (□) C_2H_6 selectivity, (○) C_2H_4 selectivity, (△) CH_3–CH_2Cl selectivity.

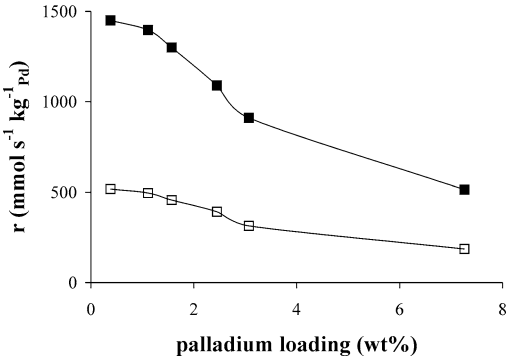

Fig. 4. Consumption rate of 1,2-dichloroethane at $T = 300$ °C (□) and $T = 350$ °C (■) as a function of palladium loading.

3.4.2. Benzene oxidation over Ag/SiO_2 and Cu/SiO_2 catalysts

Fig. 5 shows benzene conversion as a function of time and temperature for Ag1.5 and Cu1.5. Benzene conversions from 160 to 200 °C are so low for all Ag/SiO_2 and Cu/SiO_2 catalysts that these data are not presented in Fig. 5. Under experimental conditions used in the present test, benzene is oxidized in H_2O and CO_2 only.

In Fig. 5, an increase of conversion is observed when the temperature increases. However a fast deactivation is observed with Ag/SiO_2 catalysts beyond 280 °C.

In order to analyze the catalytic results, it is necessary to obtain intrinsic kinetic rates for benzene oxidation. With the experimental conditions used, the reactor is not a differential reactor because conversion is too high. The kinetic rates are obtained by considering the reactor as an integral reactor with the following assumptions: (i) for benzene oxidation on Ag/SiO_2 and Cu/SiO_2 catalysts, the kinetic rate can be expressed as: $r = k[C_6H_6]^n[O_2]^m$. For the conditions encountered in most volatile organic compound (VOC) control applications, the concentration of oxygen is always much larger than the concentration of the organic reactant (for a feed of 250 ppm benzene in air, $[O_2]/[C_6H_6] \approx 840$).

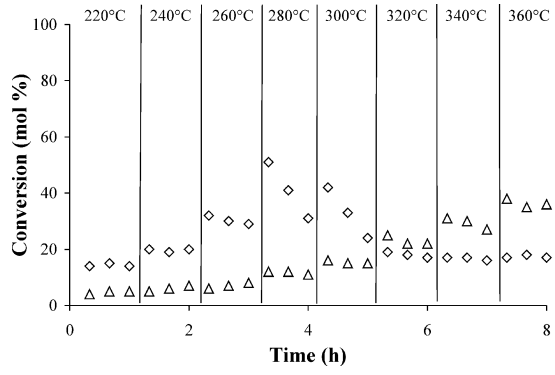

Fig. 5. Conversion of benzene as a function of time for Ag1.5 (◇) and Cu1.5 (△) samples.

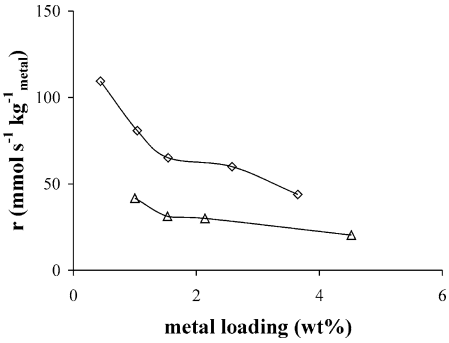

Fig. 6. Benzene consumption rate for Ag/SiO_2 catalysts at $T = 260\,^{\circ}C$ (◇) and for Cu/SiO_2 catalysts at $T = 360\,^{\circ}C$ (△) as a function of metal loading.

Thus because the oxygen partial pressure is essentially constant during the reaction, the rate observed depends only on the concentration of benzene; (ii) Gangwal et al. [33] observed a zero-order behavior for benzene on $Pt–Ni/Al_2O_3$ catalysts. Although the catalysts used in this work are different, it is, in first approximation, assumed that the kinetic rate expression is $r = k$. So the consumption rate of benzene r is calculated from chromatographic measurements of C_6H_6 concentrations in the reactor effluent using the equation

$$r = \frac{F_{B0} - F_B}{W}, \tag{3}$$

where r is the consumption rate (mmol $kg_{metal}^{-1}\,s^{-1}$), F_B is the molar flow rate of benzene at the reactor outlet (mmol s^{-1}), F_{B0} is the molar flow rate of benzene at the reactor inlet (mmol s^{-1}), and W is the metal (Ag or Cu) mass inside the reactor (kg_{metal}).

Fig. 6 presents r for benzene oxidation as a function of metal loading at 260 °C for Ag/SiO_2 catalysts and at 360 °C for Cu/SiO_2 catalysts.

4. Discussion

4.1. Formation of the gel, structure of the resulting xerogels, and nucleation phenomenon

The formation of the gels takes place in two steps. The first step consists in the formation of silica particles by hydrolysis and condensation of TEOS. The second step consists in the aggregation of silica particles to form a silica network. Those two reactions are accelerated by an increasing basicity [12]. Heinrichs et al. observed for $Pd–Ag/SiO_2$ cogelled catalysts that gel formation is faster when the amount of metal precursor and therefore when the amount of metal complexant (EDAS and AES, $NH_2–(CH_2)_3–Si–(OC_2H_5)_3$) increase [34]. In this study, when the amount of metal precursor increases and therefore when the amount of EDAS increases, the solution basicity increases (i) because either all amino groups of EDAS are not completely coordinated to a metal. Indeed, Trimmel et al. observed in Ni/SiO_2 xerogel catalysts that $Ni(acac)_2$ reacts with EDAS to give $Ni(acac)_2(EDAS)$ [35]. This present study does not establish the exact structure of complexes. Nevertheless, the formation of complexes $[Pd(acac)_x(EDAS)_y]^{n+}$, $[Ag(OAc)_x(EDAS)_y]^{n+}$, and $[Cu(OAc)_x(EDAS)_y]^{n+}$ can be supposed; x, y, and n can be different for each metal complex. Therefore, some amino groups in EDAS molecules would not be involved in metal complexation and could thus play their role of organic base; (ii) or by the growing concentration of the metal counteranion (acac or OAc), which behaves like a base and catalyzes TEOS hydrolysis and condensation. So when the amount of metal precursor increases and therefore when the basicity increases, the gelling time decreases in all series.

The weight losses after drying under vacuum, calcination, and reduction in Ag/SiO_2 and Cu/SiO_2 catalysts are smaller than in Pd/SiO_2 catalysts (Table 1). In fact, EDAS/Ag(OAc) and EDAS/$Cu(OAc)_2$ molar ratios are greater than the theoretical stoichiometric ratios to complex Ag and Cu with EDAS, whereas the EDAS/$Pd(acac)_2$ molar ratio is equal to the theoretical stoichiometric ratio to complex Pd with EDAS. Furthermore, the metal precursors are AgOAc and $Cu(OAc)_2$ for Ag/SiO_2 and Cu/SiO_2 catalysts wherever the metal precursor for Pd/SiO_2 catalysts is $Pd(acac)_2$. The ion acetate is a base stronger than the ion acetylacetonate. So these higher amounts of EDAS, Ag(OAc), or $Cu(OAc)_2$ in Ag/SiO_2 and Cu/SiO_2 catalysts increase the gel basicity and more strongly catalyze the reaction of TEOS condensation than in Pd/SiO_2 catalysts. Finally, the gelling and drying under vacuum behavior and the decomposition temperature of organic moieties depend very strongly on the kind of metal [36].

An important advantage of the cogelation method is the possibility to homogeneously disperse the catalytic metal through the whole material, for example, inside the silica particles. In the case of Pd/SiO_2 cogelled aerogel catalysts synthesized by Heinrichs et al. [6], it was suggested that this localization of the palladium inside the silica matrix was induced by a nucleation process initiated by the ligand of the palladium, namely EDAS. Nucleation by EDAS was verified by Alié et al. in xerogels without metal [8–11]. Furthermore, ^{17}O NMR spectroscopy and rheological measurements showed that the hydrolysis-condensation of EDAS is much faster than that of TEOS [37,38]. So hydrolyzed EDAS molecules can act as a nucleation agent leading to silica particles with a hydrolyzed EDAS core (where is located the metal in Pd/SiO_2 aerogel catalysts [6]) and a shell principally made of hydrolyzed TEOS.

In this work, TEM micrographs obtained for Pd/SiO_2, Ag/SiO_2, and Cu/SiO_2 catalysts show metallic particles inside microporous silica particles. To establish the nucleation mechanism by EDAS and thus by the complex $M^{n+}(EDAS)_x$, where M is palladium, silver, or copper, the relation between SiO_2 particle volume and TEOS and EDAS concentrations has been studied [6,8–11]. Thus, the volume

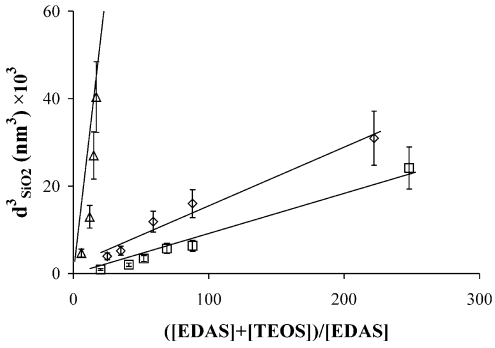

Fig. 7. Silica particle nucleation by EDAS (Pd (□), Ag (◇), and Cu (△)).

occupied of one SiO_2 particle can be expressed by

$$d^3_{SiO_2} = C\big([\text{TEOS}] + [\text{EDAS}]\big)/[\text{EDAS}], \tag{4}$$

where d_{SiO_2} is the diameter of SiO_2 particles (nm), [TEOS] and [EDAS] are the concentrations of TEOS and EDAS (mol/l), and C is a constant.

In Eq. (4), d_{SiO_2} has been measured by TEM for all the samples and is given in Table 3. The curves $d^3_{SiO_2} = f[([\text{TEOS}] + [\text{EDAS}])/[\text{EDAS}]]$ for all the samples are shown in Fig. 7. It is observed that there is effectively growth of silica particles when the ratio ([TEOS] + [EDAS])/[EDAS] increases, i.e., as [EDAS] decreases. The linearity between $d^3_{SiO_2}$ and the ratio ([TEOS] + [EDAS])/[EDAS] reinforces the hypothesis of nucleation by EDAS, since more EDAS decreases $d^3_{SiO_2}$, due to more nucleation sites. Silica particles are much larger (9.8 nm $< d_{SiO_2} <$ 60 nm, Table 3) than the monodisperse micropores of 0.8 nm detected by nitrogen adsorption in Pd/SiO_2, Ag/SiO_2, and Cu/SiO_2 xerogel catalysts (Fig. 2). Therefore, it can be reasonably assumed that those micropores are located inside the SiO_2 particles.

4.2. Dispersion and localization of metal

In Section 4.1, the nucleation mechanism by EDAS and thus by the complex $M^{n+}(EDAS)_x$ was demonstrated in all Pd/SiO_2, Ag/SiO_2, and Cu/SiO_2 catalysts. Thus, the metal crystallites with a size from 2.3 to 4.2 nm (d_{TEM1}, Table 2) are located inside the silica particles. The latter exhibit a monodisperse micropore distribution centered on a pore width of about 0.8 nm (Fig. 2). So, this characteristic width of the micropores is smaller than that of the metallic particles. It appears then that those metallic particles located inside the network of silica do not migrate outside the silica particle. These results confirm again Heinrichs et al.'s works for Pd/SiO_2 aerogel catalysts and $Pd–Ag/SiO_2$ xerogel catalysts [6,34]. Furthermore, Ruckenstein an co-workers [39,40], Zou and Gonzalez [41], and Serykh et al. [42] confirmed in Pd/SiO_2, Pt/SiO_2, and Cu/SiO_2 catalysts that the final crystallite size distribution can be strongly governed by the porous texture of silica.

Nevertheless, most of Pd/SiO_2 (except samples Pd0.4 and Pd1.1), Ag/SiO_2 (except samples Ag0.4 and Ag1.0), and Cu/SiO_2 (except samples Cu0.1, Cu1.0, and Cu1.3) xerogel catalysts exhibit larger metallic particles (with a mean diameter from 10 to 30 nm) and their number increases when the metal loading increases.

In all catalysts, the results from TEM, chemisorption (CO and O_2), and XRD (Table 2) clearly show that the greatest dispersions are obtained for low metal loadings. Several reasons can induce this phenomenon: (i) dispersion increases as the silica particle size increases (Tables 2 and 3). In Section 1, it was demonstrated that when the ratio ([TEOS] + [EDAS])/[EDAS] decreases, i.e., as [EDAS] increases, the silica particle size decreases. It then becomes possible that metal particles are not completely coated with SiO_2. Gaps would exist which allow metallic crystallites to migrate out of SiO_2 particles. The migration and coalescence mechanism can then occur; (ii) the influence of ammoniacal solution concentration on the dispersion of metal is very important. NH_3 has two functions. On the one hand, the higher the NH_3 concentration, the more complete the conversion of TEOS to SiO_2. This higher amount of SiO_2 favors a better coating of metal particles by SiO_2 and metal dispersion is therefore increased. On the other hand, metal complexation by NH_3 increases with ammonia concentration and this higher amount of free $M(NH_3)_x{}^{y+}$ (M is Pd, Ag, or Cu) is not incorporated into silica particles contrary to $M(EDAS)_x{}^{y+}$ complexes. During drying under vacuum, calcination, and reduction steps, metallic particles formed from ammonia complexes are not trapped in silica particles and can therefore migrate and undergo coalescence. The metal dispersion values then decreases. Nevertheless, in all Pd/SiO_2, Ag/SiO_2, and Cu/SiO_2 catalysts, ammonia concentration preserves a constant value. Therefore, metal complexation by NH_3 decreases proportionally when the metal loading increases. Furthermore, it is observed in Table 2 that the metal dispersion D decreases when the metal loading increases. So it is concluded that an incomplete coating of metal particles by silica has a more important effect on the metal dispersion D than metal complexation by NH_3, which could be a secondary effect.

4.3. Catalytic activity

A very important concern about cogelled catalysts is the accessibility of the active centers. Because the metal (palladium, silver, or copper) is located inside silica particles, there is a risk that it may not be accessible. The values of V_v in Table 3 show that the ability of drying under vacuum to retain porosity is high, but do not prove the accessibility of palladium, silver, or copper. Nevertheless, it is observed in Table 2 that $d_{TEM1} \cong d_{chem}$ for samples with one metal particles series (metal loading $<$ 1.5 wt%) and that $d_{TEM1} \leqslant d_{chem} \leqslant d_{TEM2}$ for samples with two metal particles series (metal loading $\geqslant$ 1.5 wt%). So in each case,

metal particle sizes obtained by CO and O_2 chemisorption measurements are related to TEM measurements. The convergence of TEM and chemisorption measurements proves metal particles located inside silica particles are completely accessible.

A high activity of a metal catalyst often calls for a large active surface area and, thus, for small particles, i.e., a high dispersion of the active phase. For all Pd/SiO_2 catalysts, it is observed from TEM, chemisorption, and XRD measurements (Table 2) that the metal dispersion, D, decreases when the metal loading increases; i.e., the metal particle size increases with the metal loading. It is observed in Fig. 4 that the specific consumption rate of 1,2-dichloroethane, r, decreases when palladium loading increases. From results in Fig. 4 and Table 2, it is concluded that Pd/SiO_2 activity decreases when palladium loading increases, i.e., when palladium dispersion decreases. So the catalytic tests of 1,2-dichloroethane hydrodechlorination with Pd/SiO_2 catalysts confirm again the evolution of metal dispersion with metal loading. The same trend is observed for Ag/SiO_2 and Cu/SiO_2 catalysts for benzene oxidation. In Table 2, the silver and copper dispersion, D, decreases when the metal loading increases, i.e., the metal particle size increases with the metal loading and in Fig. 6, the specific benzene consumption rate, r, decreases when silver and copper loading increases. From results in Fig. 6 and Table 2, it is concluded that Ag/SiO_2 and Cu/SiO_2 activity decreases when metal loading increases, i.e., when metal dispersion decreases. So the catalytic tests of benzene oxidation with Ag/SiO_2 and Cu/SiO_2 catalysts confirm again the evolution of metal dispersion with metal loading.

For benzene oxidation, Ag/SiO_2 catalysts have a greater activity than Cu/SiO_2 catalysts. In the case of metal catalysts on Fe_2O_3, Scirè et al. [43] observed that the activity toward the oxidation of volatile organic compounds (VOC) has been found to be in the order $Au/Fe_2O_3 > Ag/Fe_2O_3 > Cu/Fe_2O_3 > Fe_2O_3$ in the range of temperature investigated (100–400 °C). In this work, the same trend toward the oxidation of benzene has been found to be in the order $Ag/SiO_2 > Cu/SiO_2 > SiO_2$ (completely inactive). However in Fig. 5, a fast deactivation is observed with Ag1.5 sample from 280 °C. This deactivation could arise from a change of active site surfaces or from the disappearance of catalyst porosity. It seems that XRD *pattern* of Ag3.6 tested for 12 h at $T = 360$ °C for benzene oxidation always shows characteristic Ag–metal peaks and no AgO or Ag_2O peaks. Nevertheless, the specific surface area, S_{BET}, of fresh Ag3.6 is equal to 465 m^2/g (Table 3) and S_{BET} of tested Ag3.6 for 12 h at 360 °C is equal to 35 m^2/g. In Fig. 2, pore-size distributions over the micro- and mesopore size range are shown for fresh Ag3.6 and tested Ag3.6 samples. It is observed that micropore volume decreases very strongly in tested Ag3.6 sample. So after benzene oxidation for 12 h at $T = 360$ °C, micro- and mesoporosity of silica network disappear by pore fouling preventing benzene from reaching silver particles inside silica network. Furthermore,

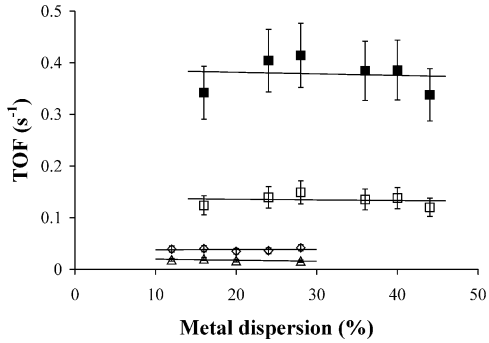

Fig. 8. TOF as a function of metal dispersion for Pd samples ($ClCH_2$–CH_2Cl hydrodechlorination) at $T = 300$ °C (□) and $T = 350$ °C (■), for Ag samples (C_6H_6 combustion) at $T = 260$ °C (◇), and for Cu samples (C_6H_6 combustion) at $T = 360$ °C (△).

O_2 chemisorption measurements of Ag1.5 samples tested for 12 h at 260 and 360 °C give values of metal dispersion, D, equal to 20 and 6%, respectively. These results indicate that the value of D for the Ag1.5 sample tested at 260 °C is equal to the value of D for the fresh Ag1.5 sample. So up to 260 °C, no deactivation is observed in Ag/SiO_2 catalysts during benzene oxidation. From 280 °C, the metal dispersion, D, of Ag1.5 sample decreases from 20% to reach the value of 6% at 360 °C. TEM analyses indicates that silver particle sizes are similar values in fresh Ag1.5 sample and Ag1.5 sample tested at 360 °C and that no sintering is observed in these samples. So the metal dispersion, D, of Ag samples tested for benzene oxidation at 360 °C is equal to 6% because O_2 molecules do not reach silver particles inside silica network because of pore fouling. No deactivation for Cu/SiO_2 catalysts is observed after benzene oxidation. In fact, S_{BET} of fresh Cu4.5 is equal to 570 m^2/g (Table 3) and S_{BET} of tested Cu4.5 is equal to 375 m^2/g.

The turnover frequency (TOF), that is, the number of molecules consumed per surface metal atom and per second, for 1,2-dichloroethane hydrodechlorination and benzene oxidation is presented in Fig. 8 as a function of metal dispersion. Nevertheless, in Fig. 5, a fast deactivation is observed for Ag/SiO_2 catalysts from 280 °C and no deactivation is observed for Cu/SiO_2 catalysts. It is for this reason that TOF is calculated at temperatures of 260 °C for Ag/SiO_2 catalysts and 360 °C for Cu/SiO_2 catalysts. It is observed in Fig. 8 that benzene oxidation TOF remains constant with metal loading and therefore metal dispersion. TOF values are equal to 0.04 s^{-1} for Ag/SiO_2 catalysts at $T = 260$ °C and are equal to 0.015 s^{-1} for Cu/SiO_2 catalysts at $T = 360$ °C. It seems that benzene oxidation is a structure-insensitive reaction too. Papaefthimiou et al. [44] measured a TOF of 0.02 s^{-1} at 180 °C for benzene oxidation with Pd/Al_2O_3 and Pt/Al_2O_3 catalysts, and in this case also, benzene oxidation is a structure-insensitive reaction. For Pd/SiO_2 catalysts, although a light deactivation is observed at 350 °C in Fig. 3, metal dispersion of fresh catalysts is used to calculate TOF at 300 and 350 °C because CO chemisorption measurements for tested Pd2.4 give a value of 24% for metal dispersion

instead of 28% for fresh Pd2.4. It is observed in Fig. 8 that TOF for 1,2-dichloroethane hydrodechlorination over Pd/SiO_2 catalysts remains constant with metal loading, and therefore metal dispersion, at $T = 300\,^{\circ}C$ and $T = 350\,^{\circ}C$. Although the structure sensitivity of C–Cl hydrogenolysis with the ensemble size concept has been pointed out by several authors [45–47], it seems in this study that 1,2-dichloroethane hydrodechlorination over Pd/SiO_2 catalysts is a structure-insensitive reaction.

5. Conclusions

The use of 3-(2-aminoethylamino)propyltrimethoxysilane (EDAS) to complex Pd, Ag, and Cu in an ethanolic solution containing TEOS and aqueous ammonia has allowed co-gelled catalysts with a hierarchic texture to be obtained. It appears that this metal complex acts as a nucleation agent for the formation of the silica particles. The examination of the texture, the metal dispersion, and its localization in co-gelled Pd/SiO_2, Ag/SiO_2, and Cu/SiO_2 catalysts leads to the following conclusion: metallic crystallites with a diameter of about 3 nm are located inside silica particles exhibiting a monodisperse microporous distribution centered on a pore width of about 0.8 nm.

Although metallic particles are located inside the silica particles, their complete accessibility, via the micropore network, has been shown. 1,2-Dichloroethane hydrodechlorination over Pd/SiO_2 catalysts mainly produces ethane and the hydrodechlorination activity decreases when palladium loading increases. Hydrodechlorination over Pd/SiO_2 catalysts is a structure-insensitive reaction with regard to the ensemble size concept. Benzene oxidation over Ag/SiO_2 and Cu/SiO_2 catalysts produces H_2O and CO_2 only and oxidation activity decreases when silver and copper loadings increase. Furthermore, it is concluded that benzene oxidation is a structure-insensitive reaction.

Finally, the synthesis method developed by Heinrichs et al. for Pd/SiO_2 aerogel catalysts and applied to monometallic xerogel catalysts in this work allows catalysts with tailored morphology and remarkable catalytic characteristics to be obtained.

Acknowledgments

The authors thank the Centre d'Enseignement et de Recherche des Macromolécules, C.E.R.M., from the University of Liège for TEM analysis, and the Laboratoire de Chimie Inorganique Structurale from the University of Liège for XRD analysis. S.L. is grateful to the Belgian Fonds pour la Formation à la Recherche dans l'Industrie et dans l'Agriculture, F.R.I.A., for a PhD grant. The authors also thank the Belgian Fonds National de la Recherche Scientifique, the Fonds de Bay, the Fonds de Recherche Fondamentale et Collective, the Ministère de la Région Wallonne, and the Ministère de la Communauté Française (Action de Recherche Concertée) for their financial support.

References

[1] L.A.M. Hermans, J.W. Geus, Stud. Surf. Sci. Catal. 3 (1979) 113.
[2] B. Breitscheidel, J. Zieder, U. Schubert, Chem. Mater. 3 (1991) 559.
[3] U. Schubert, New J. Chem. 18 (1994) 1049.
[4] W. Mörke, R. Lamber, U. Schubert, B. Breitscheidel, Chem. Mater. 6 (1994) 1659.
[5] A. Kaiser, C. Görsmann, U. Schubert, J. Sol–Gel Sci. Technol. 8 (1997) 795.
[6] B. Heinrichs, F. Noville, J.-P. Pirard, J. Catal. 170 (1997) 366.
[7] B. Heinrichs, J.-P. Schoebrechts, J.-P. Pirard, AIChE J. 47 (2001) 1866.
[8] C. Alié, R. Pirard, A.J. Lecloux, J.-P. Pirard, J. Non-Cryst. Solids 246 (1999) 216.
[9] C. Alié, A. Benhaddou, R. Pirard, A.J. Lecloux, J.-P. Pirard, J. Non-Cryst. Solids 270 (2000) 77.
[10] C. Alié, R. Pirard, A.J. Lecloux, J.-P. Pirard, J. Non-Cryst. Solids 285 (2001) 135.
[11] C. Alié, F. Ferauche, R. Pirard, A.J. Lecloux, J.-P. Pirard, J. Non-Cryst. Solids 289 (2001) 88.
[12] C.J. Brinker, G.W. Scherer, Sol–Gel Science: The Physics and Chemistry of Sol–Gel Processing, Academic Press, San Diego, 1990.
[13] J. Rouquerol, D. Avnir, C.W. Fairbridge, D.H. Everett, J.H. Haynes, N. Pernicone, J.D.F. Ramsay, K.S.W. Sing, K.K. Unger, Pure Appl. Chem. 66 (1994) 1739.
[14] D.J.C. Yates, J.H. Sinfelt, J. Catal. 8 (1967) 348.
[15] J.J.F. Scholten, J.A. Konvalinka, F.W. Beekman, J. Catal. 28 (1973) 209.
[16] S. Razi Seyedmonir, D.E. Strohmayer, G.L. Geoffroy, M.A. Vannice, J. Catal. 87 (1984) 424.
[17] J.H. Sinfelt, Bimetallic Catalysts—Discoveries, Concepts, and Applications, Wiley, New York, 1983.
[18] J.E. Benson, H.S. Hwang, M. Boudart, J. Catal. 30 (1973) 146.
[19] G. Bergeret, P. Gallezot, in: G. Ertl, H. Knözinger, J. Weitkamp (Eds.), Handbook of Heterogeneous Catalysis, Wiley–VCH, Weinheim, 1997, p. 439.
[20] J.R. Anderson, Structure of Metallic Catalysts, Academic Press, London, 1975.
[21] E. Iglesia, M. Boudart, J. Catal. 81 (1983) 204.
[22] D. Cormack, J. Pritchard, R.L. Moss, J. Catal. 37 (1975) 548.
[23] J.J.F. Scholten, A. Van Montfoort, J. Catal. 1 (1962) 85.
[24] S. Ichikawa, H. Poppa, M. Boudart, J. Catal. 91 (1985) 1.
[25] J.S. Rieck, A.T. Bell, J. Catal. 103 (1987) 46.
[26] C.L.M. Joyal, J.B. Butt, J. Chem. Soc., Faraday Trans. 83 (1987) 2757.
[27] R.P. Eischens, S.A. Francis, W.A. Pliskin, J. Phys. Chem. 60 (1956) 194.
[28] A.W. Czanderna, J. Phys. Chem. 68 (1964) 2765.
[29] W.M.H. Sachtler, C. Backse, R.A. van Santen, Catal. Rev. Sci. Eng. 23 (1981) 127.
[30] Y.-P. Wang, C.-T. Yeh, S.-H. Chien, J. Chem. Soc., Faraday Trans. 1 85 (1989) 2199.
[31] A.A. Vasilevich, G.P. Shpiro, A.M. Alekseev, T.A. Semenova, M.I. Markina, T.A. Vasil'eva, O.G. Budkina, Kinet. Katal. 16 (1975) 1571.
[32] M. Yamane, in: L.C. Klein (Ed.), Sol–Gel Technology for Thin Films, Fibers, Preforms, Electronics and Specialty Shapes, Noyes, Park Ridge, NJ, 1988, p. 200.
[33] S.K. Gangwal, M.E. Mullins, J.J. Spivey, P.R. Caffrey, Appl. Catal. 36 (1988) 231.
[34] B. Heinrichs, P. Delhez, J.-P. Schoebrechts, J.-P. Pirard, J. Catal. 172 (1997) 322.
[35] G. Trimmel, C. Lembacher, G. Kickelbick, U. Schubert, New J. Chem. 26 (2002) 759.
[36] G. Trimmel, U. Schubert, J. Non-Cryst. Solids 296 (2001) 188.

[37] C. Alié, J.-P. Pirard, J. Non-Cryst. Solids 320 (2003) 21.
[38] C. Alié, R. Pirard, J.-P. Pirard, J. Non-Cryst. Solids 320 (2003) 31.
[39] E. Ruckenstein, D.B. Dadyburjor, J. Catal. 48 (1977) 73.
[40] E. Ruckenstein, B. Pulvermacher, J. Catal. 37 (1975) 416.
[41] W. Zou, R.D. Gonzalez, Appl. Catal. 126 (1995) 351.
[42] A.I. Serykh, O.P. Tkachenko, V.Y. Borovkov, V.B. Kazansky, K.M. Minachev, C. Hippe, N.I. Jaeger, G. Schulz-Ekloff, Phys. Chem. Chem. Phys. 2 (2000) 2667.
[43] S. Scirè, S. Minicŏ, C. Crisafulli, S. Galvagno, Catal. Commun. 2 (2001) 229.
[44] P. Papaefthimiou, T. Ioannides, X.E. Verykios, Appl. Catal. B 13 (1997) 175.
[45] B. Coq, G. Ferrat, F. Figueras, J. Catal. 101 (1986) 434.
[46] P. Fouilloux, G. Cordier, Y. Colleuille, Stud. Surf. Sci. Catal. 11 (1982) 369.
[47] Y. Soma-Noto, W.M.H. Sachtler, J. Catal. 32 (1974) 315.